Treatment Optimization for Tumor Growth by Ordinary Differential Equations

Kenneth Chan[1], Chiu-Yen Kao[1], Jennifer Gordinier[1], and Katherine Ganden[#]

[1]Pine Crest School, Claremont McKenna College
[#]Advisor

ABSTRACT

Cancer is the second leading cause of death worldwide and with the disease having over 200 variations, it has not been cured yet despite being the priority of the medical field for decades. Due to the difficulty of human subject research, animal studies, e.g., mouse and Chinese hamster V79 tumors have been widely used to test the modeling of tumor growth due to their dynamic nature and ability to grow to high volumes within short periods of time. Mathematical models, including ordinary differential equations (ODEs), have been utilized to model tumor growth and study treatment of cancer. With most current models being selected only for mathematical convenience, recent studies have been focusing on determining the optimal treatment schedule for the most popular existing treatments of chemotherapy and radiation therapy. In this paper, three of the most established ODE models: the Gompertz, Von Bertalanffy, and logistic models are utilized to analyze which model most accurately fits existing tumor growth data for the Chinese Hamster V79 fibroblast tumor, various forms of immunodeficient mice tumors, and glioblastoma based on the minimization of the normalized mean squared error (NMSE). Next, the ODEs themselves were modified to simulate the growth of the tumors when exposed to treatment and determined which treatment schedule produced the lowest final volume of the tumors. The results of this research identify the optimal treatment schedules based on data from all three ODE models and also determine the ODE models that produce curves that most precisely fit the datasets.

Introduction

Cancerous tumors continue to cause the second-highest number of deaths worldwide. Chemotherapy and radiation therapy are the most common forms of treatment, with treatment schedules varying between patients and the types of tumors.

ODEs have been a prevalent form of mathematical modeling with regards to its applications in tumor growth. However, there has been widespread discrepancy amongst previous literature in determining which ODE model is the most accurate when fitted to tumor growth data. In this paper, we consider various forms of mice and hamster tumors as well as glioblastoma, a grade 4 malignant brain tumor that is currently one of the most aggressive and widespread forms of cancer. We studied the tumor growth behavior under a treatment designed to simulate chemotherapy, which targets the tumor at a single location.

The Bertalanffy, Gompertz, and logistic models have been previously studied in the context of tumor growth and have been established as three of the most optimal ODEs. Jue Wang utilized these three ODEs to model the growth of a Chinese Hamster V79 Fibroblast and Mouse CM.37 T.1 tumor, determining the optimal parameters that would produce a minimum NMSE value (Wang, 2018).

In this paper, we analyze the efficacy of the same three ODE models in producing a best-fit curve for each of our 9 datasets (Wang, 2018; Gaddy et al., 2017; Staat, 2020). Further, we alter the ODEs to simulate tumor behavior under our treatment function, as defined within our models. We consider 21 variations of a 7-day treatment schedule with 5 days of active and 2 days of inactive treatment. Ultimately, our research contributes to the ongoing discussion of the best-fitting ODE model and determines the optimal treatment schedule to limit the onset of tumor growth.

In the first section, we review three different tumor growth models and their corresponding type I and type II treatment, each with 21 variations. In the next section, we discuss a theoretical result regarding the constant final tumor volume with a fixed total treatment amount. Computational approaches are then described. Numerical experiments including least NMSE fitting and most effective treatment are presented in the next section, and we conclude in the final section with a discussion of treatment results.

Tumor Growth Models

Here we briefly review three well-established and popular methods that have been used to predict tumor growth: the logistic, Bertalanffy, and Gompertz ODE models. We then modify them to incorporate the treatment.

Tumor Growth Models Without Treatment

The logistic model is represented by the following differential equation, in which there is a linear decrease of the growth rate and a carrying capacity of b (Vogels et al., 1838).

Equation 1: Logistic Model:

$$\frac{dV}{dt} = aV(1 - \frac{V}{b})$$

The carrying capacity is specifically defined as the maximum tumor volume in the context of our research. This maximum tumor volume occurs due to increasing competition over nutrients as the tumor grows and a lack of blood vessels to sustain the proliferation of tumor cells indefinitely.

Equation 2: Bertalanffy Model:

$$\frac{dV}{dt} = aV^{2/3} - bV$$

The above equation is the Bertalanffy model. The model was created by Ludwig Bertalanffy in 1957 to model organism growth (Von Bertalanffy, 1957). The first term of the ODE has an order of ⅔ due to the surface rule model, which assumes that cell growth is proportional to its surface area, which defines the amount of energy/nutrients a cell can absorb. Additionally, the Bertalanffy model accounts for both cell synthesis and death through the two terms of the equation, each having its respective parameter of a or b (Murphy et al., 2016). Lastly, the Gompertz model, represented by the following ODE, was initially created by Benjamin Gompertz in 1825 to model human mortality and determine the value of life insurances (Kirkwood, 2015).

Equation 3: Gompertz Model:

$$\frac{dV}{dt} = V(a - b \ln V)$$

The model was later applied to breast and lung cancer growth and has been an integral part of the mathematical modeling of various types of tumors. The ODE presents an exponential decay of the growth rate as well as a maximum tumor size (Murphy et al., 2016).

Treatment

Treatment Models
In order to count for the treatment, we modify the aforementioned models to

Equation 4: Logistic Model for Type I Treatment:

$$\frac{dV}{dt} = aV\left(1 - \frac{V}{b}\right) - R \times C_{max} \times aV(1 - \frac{V}{b})$$

Equation 5: Bertalanffy Model for Type I Treatment:

$$\frac{dV}{dt} = aV^{2/3} - bV - R \times C_{max} \times (aV^{2/3} - bV)$$

Equation 6: Gompertz Model for Type I Treatment:

$$\frac{dV}{dt} = V(a - b\ln V) - R \times C_{max} \times V(a - b\ln V)$$

for type I treatment and

Equation 7: Logistic Model for Type II Treatment:

$$\frac{dV}{dt} = aV\left(1 - \frac{V}{b}\right) - R \times C_{max} \times aV$$

Equation 8: Bertalanffy Model for Type II Treatment:

$$\frac{dV}{dt} = aV^{2/3} - bV - R \times C_{max} \times aV^{2/3}$$

Equation 9: Gompertz Model for Type II Treatment:

$$\frac{dV}{dt} = V(a - b\ln V) - R \times C_{max} \times aV$$

for type II treatment, where in both treatments, the constant C_{max} indicates the strength of the treatment and *R(t)* is an on-off function which specifies the treatment activity. The type I treatment introduces an overall degradation based on the growth rate of the original model. Meanwhile, type II treatment represents a linear decay for the logistic and Gompertz models and a degradation according to the surface rule for the Bertalanffy model.

Treatment Schedule
When the treatment was inactive/active, the R value was set to 0/1 accordingly. Mathematically, the ODE remains unchanged when R is 0, thus accounting for the inactivity of the treatment. Meanwhile, when R is 1, the treatment is activated with a degradation proportional to C_{max}. The C_{max} value served as a measurement of the strength of the simulated treatment and was kept constant at 0.75 for all considered treatment schedules amongst the three ODE models. Here, the treatment schedule was standardized to a 7-day period, with 5 days of active treatment and 2 days where the treatment was inactive. Thus, combinatorics yielded 21 possible treatment schedules that maintained the pattern of 5 active days and 2 inactive days. To account for all possible treatment schedules, the treatment function

was programmed to consider all 21 different treatment schedules, adjusting the R values accordingly as a function of time. The treatment schedule was visually represented in the treatment graphs with a subplot indicating when the treatment was active over a 7-day period (Table 1). For the purpose of the research, the location of the treatment was not considered, which could be a factor for treatment such as radiation therapy. Instead, the sole focus of our analysis was the treatment schedule.

Table 1. The 21 treatment schedules across a 7-day period, with 0 denoting inactive treatment and 1 denoting active treatment.

	Days						
	1	2	3	4	5	6	7
1	0	0	1	1	1	1	1
2	0	1	0	1	1	1	1
3	0	1	1	0	1	1	1
4	0	1	1	1	0	1	1
5	0	1	1	1	1	0	1
6	0	1	1	1	1	1	0
7	1	0	0	1	1	1	1
8	1	0	1	0	1	1	1
9	1	0	1	1	0	1	1
10	1	0	1	1	1	0	1
11	1	0	1	1	1	1	0
12	1	1	0	0	1	1	11
13	1	1	0	1	0	1	1
14	1	1	0	1	1	0	1
15	1	1	0	1	1	1	0
16	1	1	1	0	0	1	1
17	1	1	1	0	1	0	1
18	1	1	1	0	1	1	0
19	1	1	1	1	0	0	1
20	1	1	1	1	0	1	0
21	1	1	1	1	1	0	0

(Left side vertical label: Treatment Schedule)

MathematicalAnalysis

When the ODE model is separable, the equation can be anti-differentiated to obtain the final tumor volume defined in an implicit manner. We will show the final volume is identical across treatments with the same number of active days. The following serves as mathematical justification for the equivalent final tumor volume across different treatment schedules.

The ODE models utilized can be stated in the general form as follows,

Equation 10: Theorem 1:

$$\frac{dV}{dt} = \frac{1}{f(V)}(1 - R(t)C_{max})$$

where *f(V)* varies with respect to different models. For example, the logistic model has

Equation 11: Theorem 1:

$$\frac{1}{f(V)} = aV\left(1 - \frac{V}{b}\right).$$

By separation of variables, we have

Equation 12: Theorem 1:

$$f(V)\frac{dV}{dt} = 1 - R(t)C_{max}.$$

After integrating both sides from t_0 to T, denoting $V(t_0)$ as V_0, and assuming that the anti-derivative of f(V) is F(V), we have

Equations 13/14: Theorem 1:

$$F\big(V(T)\big) - F(V_0) = \int_0^T (1 - R(t)C_{max})dt$$
$$= T - C_{max}\int_0^T \big(R(t)\big)dt.$$

If T is given and $\int_0^T \big(R(t)\big)dt$ is a constant, the final volume *V(t)* is implicitly determined by the above equation. This concludes that the final volume depends on the integration of the treatment as determined by the number of active days. Therefore, if the total number of active days is the same, the final tumor volume will be identical. On the other hand, the ODE models for type II treatment are non-separable, preventing us from drawing this conclusion. Instead, we will determine the final volume with a numerical approach to be discussed later.

NMSEFitting

In this section, we will discuss the datasets, numerical approach to solve the ODEs, and the fitting performed to minimize the NMSE. With the use of numerical methods implemented by Python, the goal of our research was to find the model that fit our existing tumor growth data the most effectively and use the model to optimize the treatment schedule for each type of tumor. We will first introduce the datasets that were used. We shall then discuss the mathematical methods implemented in our Python code and the utilization of the NMSE to measure fitting accuracy. Finally, we will discuss the results of the model-fitting and draw conclusions on the best-fit model for each dataset.

Dataset

We use nine online datasets which display the tumor volume (mm3) as a function of time (days) for the tumors of Mouse CM.37 T.1, Chinese hamster V79 fibroblast, glioblastoma, SCID (severe combined immunodeficiency), NSG (nonobese SCID gamma), nude (nu/nu), and BALB/Slc-nu/nu mice. The datasets are shown in the tables in the Appendix.

ODE Solver

In order to find the solution of the ODEs numerically, the odeint package from scipy.integrate was utilized. The odeint library includes a variety of methods from the Runge-Kutta family, with Euler's method being the simplest one available. In order to maximize the accuracy of the ODE graphs, Python was utilized in order to solve the ODEs over small step sizes that could only be produced within the code. The methods within the Runge-Kutta family are generally characterized as controlled steppers or dense-output-steppers. Controlled-steppers perform step-size control, in which they can adjust the step-size between intervals to achieve maximum accuracy. Dense-output-steppers perform continuous interpolation between consecutive time intervals rather than only during the steps themselves. With Euler's method being a first order stepper, the Runge-Kutta methods were optimal for achieving a higher level of accuracy for the ODE graphs as they were higher order methods that allowed for more frequent interpolation within step sizes. The code for the ODE models employed the Runge-Kutta 4 method, the most renowned algorithm that utilizes a fixed step size and provides a robust approach to develop the approximation. In this paper, the Runge-Kutta 4 method is used.

Fitting

In order to align the curves produced by the ODE models with the tumor growth datasets, the values of the parameters a and b were determined in equations 1, 2, and 3 discussed in section 3.1. The parameter values were optimized such that the NMSE of the ODE when compared with the data was at a minimum value (closest to 0). The NMSE of a function is a normalized form of its sum of squared residuals (SSR), meaning that the sum of squared residuals is then divided by the sum of all the actual y values presented by the data. The y_i term represents the actual data values while the $ypred_i$ represents the predicted values. Both calculations are shown below.

Equation 15: SSR:

$$SSR = \sum_{0}^{i}(y_i - ypred_i)^2$$

Equation 16: NMSE:

$$NMSE = \frac{\sum_{0}^{i}(y_i - ypred_i)^2}{\sum_{0}^{i}y_i^2}$$

To perform the parameter optimization, the code employed the minimize package from the scipy.optimize library within Python. The minimize function utilized Powell's Method, which is an algorithm that generates a bi-directional search to find the local minimum of a function. Powell's Method was specified within the calling of the odeint function and returned the minimum NMSE values for each ODE model and the corresponding parameter values. The resulting parameter values and the corresponding NMSE values for each ODE model are shown in Figure 1 below. For the purpose of the model-fitting, the x-values were subtracted by 3.46 for the Chinese hamster V79 fibroblast dataset such that the data begins when time is equal to zero days. Therefore, the NMSE values shown below may differ from existing literature involving the same datasets due to a similar shift in the data coordinates.

Chinese Hamster V79 Fibroblast
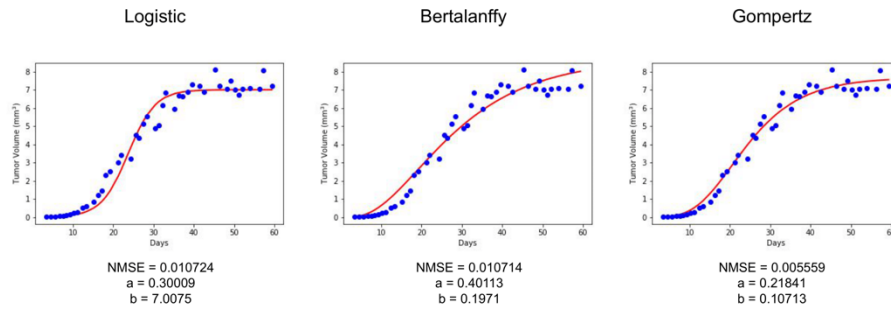
Glioblastoma
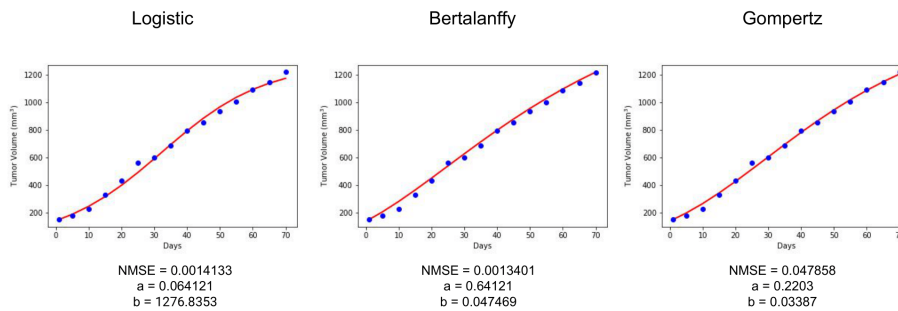
NOD/SCID Mice
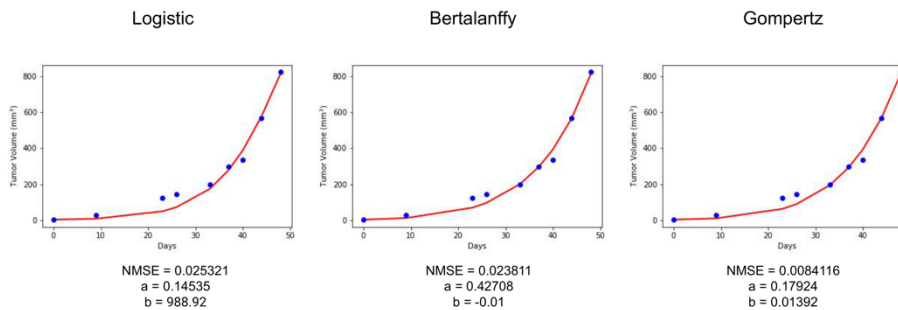
BALB/Slc-nu/nu Mice
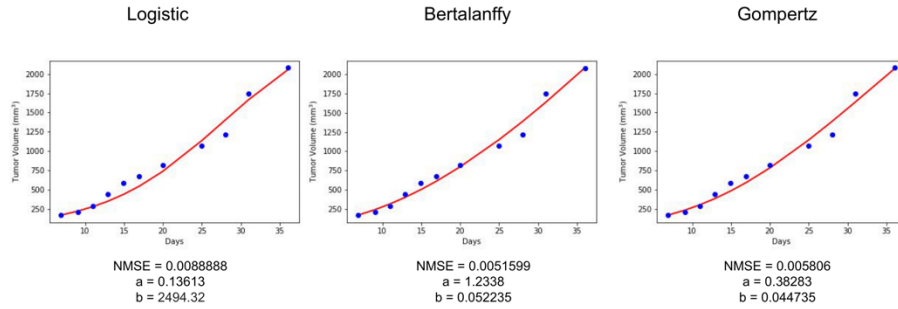
nu/nu Mice
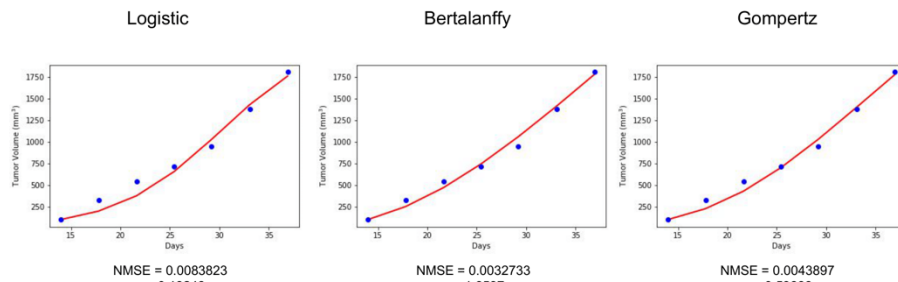
SCID Mice
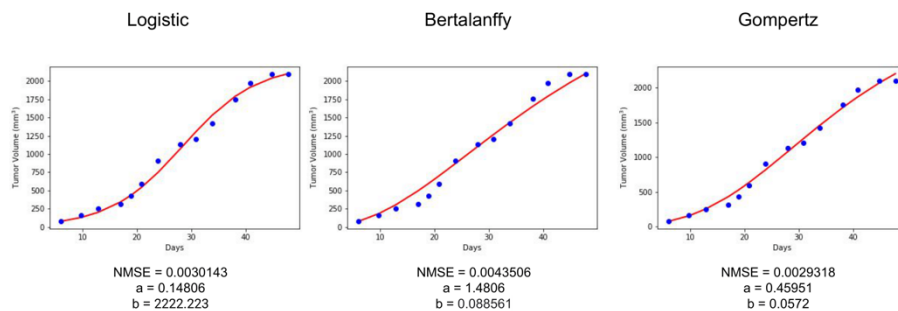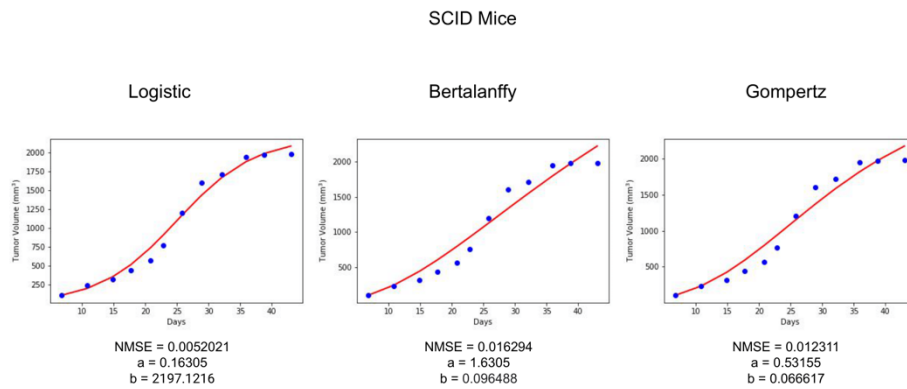
Figure 1. The fitted logistic, Bertalanffy, and Gompertz models for all datasets.
Fitting Results/Discussion

After analyzing the NMSEs produced by each of the ODE models, the best-fitting models were determined for the datasets. The results are shown in table 2 below.

Table 2. The best fit-models that produced the lowest NMSE value for each of the 9 datasets.

Dataset	Best-fit ODE Model
Mouse CM.37 T.1	Logistic
Chinese Hamster V79 Fibroblast	Gompertz
Glioblastoma	Bertalanffy
NOD/SCID	Gompertz
NSG Immunodeficient	Gompertz
BALB/Slc/nu-nu	Bertalanffy
nu/nu	Bertalanffy
SCID	Gompertz
SCID	Logistic

TreatmentResults

The adjusted ODEs for type I and type II treatment were solved with the optimized parameters that were obtained in the previous section. The best-fit ODE models displayed in figure 2 were utilized to draw conclusions regarding the efficacy of each treatment schedule in limiting tumor growth. Thus, the comparison of the NMSE values produced was crucial in ensuring that the ODE model selected to analyze results would yield the highest accuracy and thus validate our findings. The treatment curves were then plotted and fitted for each of the 21 7-day treatment schedules, 2 forms of treatment, 3 ODE models, and 9 datasets, resulting in 1134 total figures. All figures were produced with the use of the matplotlib.pyplot, which was imported as plt into the code. As mentioned, the treatment curves were

generated with the introduction of a degradation term determined by R and Cmax. To analyze the results across the 1134 figures, 18 scatter plots were created, one for each dataset and form of treatment, that displayed the final tumor volume (mm³) as a function of the treatment schedule, Rid. The scatter plots are shown in figure 2 below.

Type I

Treatment   **Type II Treatment**

Mouse CM.37 T.1
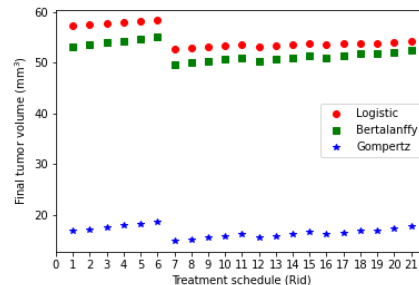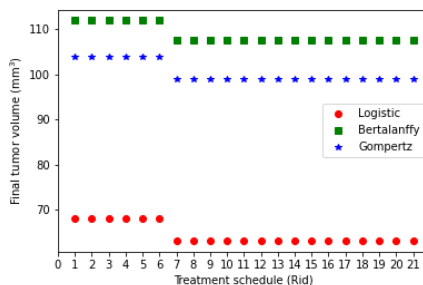
Chinese Hamster V79 Fibro-blast
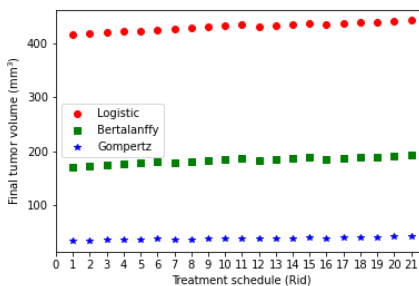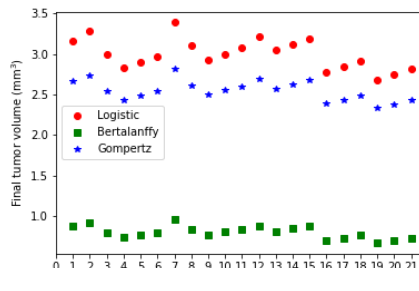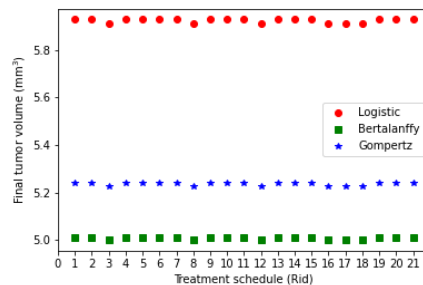
Glioblastoma
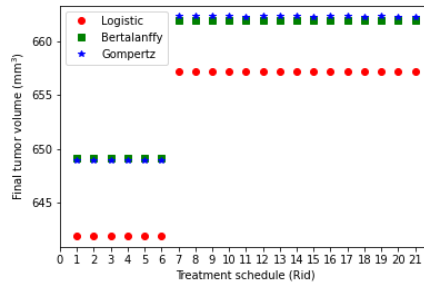
NOD/SCID
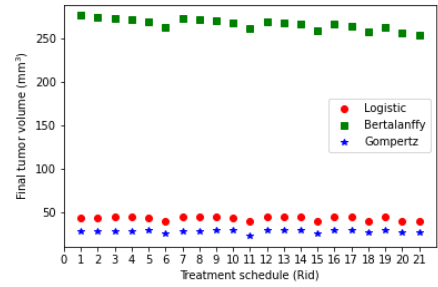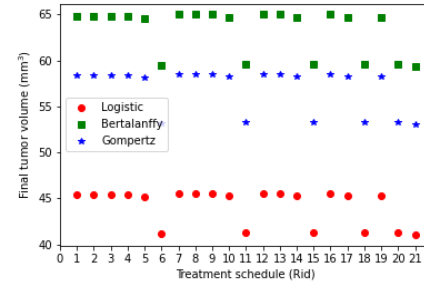
NSG Immunodeficient
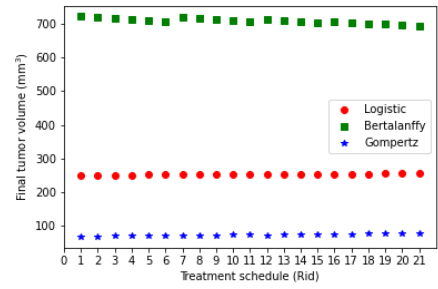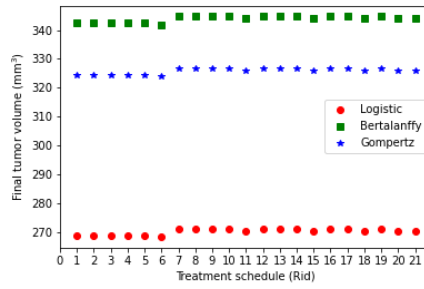
BALB/Slc-nu/nu
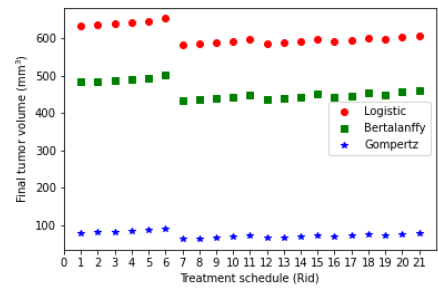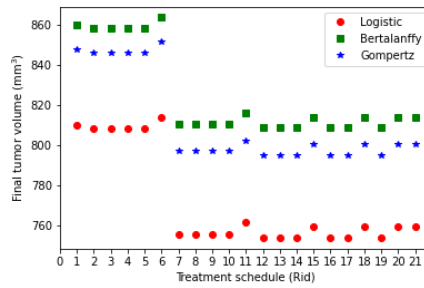
nu/nu
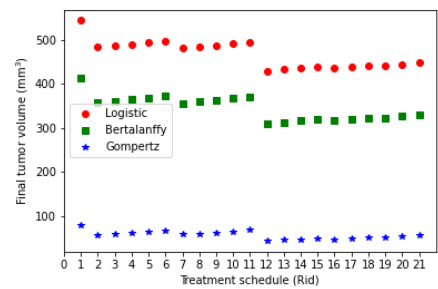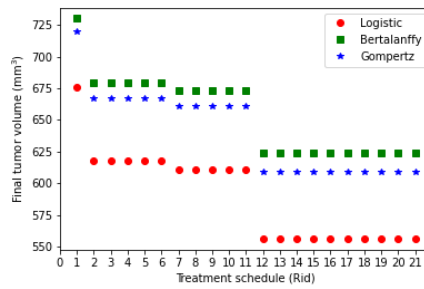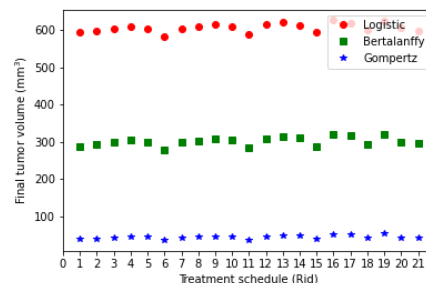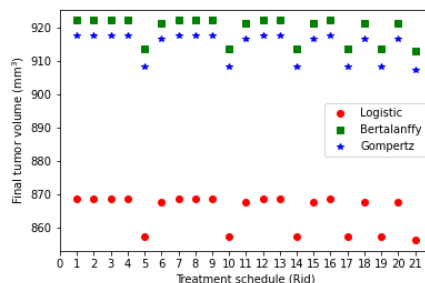
SCID

SCID
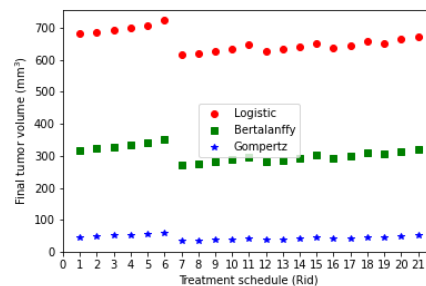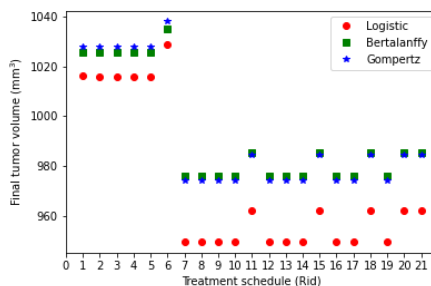
Figure 2. The scatter plots display the final tumor volume as a function of the treatment schedule, Rid. Predicted tumor volumes are shown for each of the three ODE models.

Conclusions regarding the efficacy of each treatment schedule on limiting the final tumor volume were made based on the models that produced the lowest NMSE for each dataset. For type I treatment, the final tumor volume was a direct result of the number of active treatment days. The Mouse CM. 37 T.1 dataset exemplifies this pattern. While the data was collected over a period of 78 days, we can assume that all treatment schedules return an identical volume after 77 days by the theorem discussed in section 2, since all schedules had 55 days of active treatment. Thus, the only discrepancy in final tumor volume between schedules was caused by the treatment activity on the 78th day. With treatment schedules 1-6 inactivating treatment on the 78th day and schedules 7-21 activating the treatment on this day, the first 6 treatment schedules will still have 55 days of active treatment while the last 15 will have 56 days. The results confirm the correlation between active treatment days and tumor volume as treatment schedules 1-6 returned a higher tumor volume than schedules 7-21. On the other hand, the ODEs utilized to simulate type II treatment were non-separable, preventing the application of the theorem previously discussed. Thus, more variation in final tumor volume across schedules was observed and no clear pattern was established for type II treatment. The individual treatment graphs for each treatment schedule including the fitted curve, treatment curve, and the original data points are displayed in the Appendix. Treatment schedules are represented in the subplot below each graph of the fitted and treatment curves. Table 3 displays the least and most effective treatment schedules for each tumor and type of treatment.

Table 3. The final volumes under the least and most effective treatment schedules as predicted by the best-fitting ODE model for each dataset. The most effective are shaded in green while the least-effective are shaded in red.

Tumor, Treatment Schedule(s), Type I Tumor, Treatment Schedule(s), Type II	Final Volume (mm³)
	63.0729

Mouse CM.37 T.1, Treatment Schedule 7-21 Mouse CM.37 T.1, Treatment Schedule 7	52.7949
Mouse CM.37 T.1, Treatment Schedule 1-6 Mouse CM.37 T.1, Treatment Schedule 6	67.9719 58.3273
Chinese Hamster V79 Fibroblast, Treatment Schedules 3, 8, 12, 16, 17, 18 Chinese Hamster V79 Fibroblast, Treatment Schedule 19	5.2264 2.3321
Chinese Hamster V79 Fibroblast, Treatment Schedules 1, 2, 4, 5, 6, 7, 9, 10, 11, 13, 14, 15, 19, 20, 21 Chinese Hamster V79 Fibroblast, Treatment Schedule 7	5.2393 2.8105
Glioblastoma, Treatment Schedules 1-6 Glioblastoma, Treatment Schedule 1	649.165 162.623
Glioblastoma, Treatment Schedules 7-21 Glioblastoma, Treatment Schedule 21	661.983 187.682
NOD/SCID, Treatment Schedule 21 NOD/SCID, Treatment Schedule 11	53.095 22.886
NOD/SCID, Treatment Schedules 7, 8, 9, 12, 13, 16 NOD/SCID, Treatment Schedule 19	58.511 29.990

NSG Immunodeficient, Treatment Schedule 6	323.939
NSG Immunodeficient, Treatment Schedule 1	66.540
NSG Immunodeficient, Treatment Schedules 7, 8, 9, 10, 12, 13, 14, 16, 17, 19	326.688
NSG Immunodeficient, Treatment Schedule 21	77.906
BALB/Slc-nu/nu, Treatment Schedules 12, 13, 14, 16, 17, 19	809.047
BALB/Slc-nu/nu, Treatment Schedule 7	436.0474
BALB/Slc-nu/nu, Treatment Schedule 6	863.911
BALB/Slc-nu/nu, Treatment Schedule 6	502.3434
nu/nu, Treatment Schedules 12-21	623.6939
nu/nu, Treatment Schedule 12	310.1888
nu/nu, Treatment Schedule 1	730.1343
nu/nu, Treatment Schedule 1	412.1961
SCID, Treatment Schedule 21	907.4536
SCID, Treatment Schedule 6	36.0899
SCID, Treatment Schedule 1, 2, 3, 4, 7, 8, 9, 12, 13, 16	917.5078
SCID, Treatment Schedule 19	53.0116
SCID, Treatment Schedules 12, 13, 14, 16, 17, 19	949.546
SCID, Treatment Schedule 7	615.010
SCID, Treatment Schedule 6	1028.649

SCID, Treatment Schedule 6	723.184

Conclusion/Future Research

Ultimately, the results determined that when C_{max} was kept constant at a value of 0.75, the optimal treatment schedules differed between the types of tumors, suggesting that no single schedule can be universally accepted as most effective in limiting tumor growth. The results are limited by the simplification of the treatment to a single constant, C_{max}. Therefore, forms of treatment such as radiotherapy were not accounted for, as they can target tumor growth at several different locations. The ODE models assumed treatment was targeted at a single location and partial differential equations (PDEs) would have to be employed in order to factor in multiple different locations. Additionally, with regards to chemotherapy, the research did not account for the quantification of drug doses that correlate to the C_{max} constant. Lastly, the side effects to patients that would be subjected to the assumed treatments were not considered. These limitations exist as a result of the mathematical modeling being strictly computational, without any physical or medical testing having been performed. The future direction of the research will be to incorporate a wider range of datasets to improve the reliability of the model-fitting results and allow for the analysis of a greater variety of tumor growth behavior. Additionally, a major aspect of the future direction of the research involves applying the models in a laboratory setting and determining how to quantify chemotherapy relative to the C_{max} value. Further, another objective will be to determine whether type I or type II treatment is more applicable to real-life uses of chemotherapy to target tumor growth. The final stage of the research would involve the experimental testing of the treatment on mouse and hamster subjects and the subsequent analysis of their tumor growth.

Acknowledgements

References

Meaney, C., Stastna, M., Kardar, M., & Kohandel, M. (2019). Spatial optimization for radiation therapy of brain tumours. *PloS one*, *14*(6), e0217354. https://doi.org/10.1371/journal.pone.0217354

Murphy, H., Jaafari, H., & Dobrovolny, H. M. (2016). Differences in predictions of ODE models of tumor growth: a cautionary example. *BMC cancer*, *16*, 163. https://doi.org/10.1186/s12885-016-2164-x

Wang J. STUDENT VERSION Modeling Cancer Growth with Differential Equations. www.semanticscholar.org. Published 2018. Accessed December 1, 2022. https://www.semanticscholar.org/paper/STUDENT-VERSION-Modeling-Cancer-Growth-with-Wang/9291329883b92690de01b4237e20b966f63d904d

Yousefnezhad, Mohsen, Kao, Chiu-Yen, & Mohammadi, Seyyed Abbas. *Optimal Chemotherapy for Brain Tumor Growth in a Reaction-Diffusion Model. SIAM Journal on Applied Mathematics*, *81* (3). Retrieved from https://par.nsf.gov/biblio/10322732. https://doi.org/10.1137/20M135995X

Corwin, D., Holdsworth, C., Rockne, R. C., Trister, A. D., Mrugala, M. M., Rockhill, J. K., Stewart, R. D., Phillips, M., & Swanson, K. R. (2013). Toward patient-specific, biologically optimized radiation therapy plans for the treatment of glioblastoma. *PloS one*, *8*(11), e79115. https://doi.org/10.1371/journal.pone.0079115

Seidlitz, T., Chen, Y. T., Uhlemann, H., Schölch, S., Kochall, S., Merker, S. R., Klimova, A., Hennig, A., Schweitzer, C., Pape, K., Baretton, G. B., Welsch, T., Aust, D. E., Weitz, J., Koo, B. K., & Stange, D. E. (2019). Mouse Models of Human Gastric Cancer Subtypes With Stomach-Specific CreERT2-Mediated Pathway Alterations. *Gastroenterology*, *157*(6), 1599–1614.e2. https://doi.org/10.1053/j.gastro.2019.09.026

Mulansky, M., & Ahnert, K. (n.d.). *Odeint Library*. Scholarpedia. Retrieved January 19, 2023, from http://www.scholarpedia.org/article/Odeint_library

Vassiliadis, V. S., & Conejeros, R. (1970, January 1). *Powell method*. SpringerLink. Retrieved January 19, 2023, from https://link.springer.com/referenceworkentry/10.1007/0-306-48332-7_393#citeas

Gaddy, T. D., Wu, Q., Arnheim, A. D., & Finley, S. D. (2017). Mechanistic modeling quantifies the influence of tumor growth kinetics on the response to anti-angiogenic treatment. *PLoS computational biology*, *13*(12), e1005874. https://doi.org/10.1371/journal.pcbi.1005874

Staat, C. (n.d.). *(PDF) finding the growth rate of a tumor - researchgate*. Finding the Growth Rate of a Tumor. https://www.researchgate.net/publication/339577784_Finding_the_Growth_Rate_of_a_Tumor

Vogels, M., Zoeckler, R., Stasiw, D.M. *et al.* P. F. Verhulst's "notice sur la loi que la populations suit dans son accroissement" from correspondence mathematique et physique. Ghent, vol. X, 1838. *J Biol Phys* **3**, 183–192 (1975). https://doi.org/10.1007/BF02309004

VON BERTALANFFY L. (1957). Quantitative laws in metabolism and growth. *The Quarterly review of biology*, *32*(3), 217–231. https://doi.org/10.1086/401873

Kirkwood T. B. (2015). Deciphering death: a commentary on Gompertz (1825) 'On the nature of the function expressive of the law of human mortality, and on a new mode of determining the value of life contingencies'. *Philosophical transactions of the Royal Society of London. Series B, Biological sciences*, *370*(1666), 20140379. https://doi.org/10.1098/rstb.2014.0379